Local versus systemic control of bone and skeletal muscle mass by components of the transforming growth factor-β signaling pathway

Yewei Liu[a], Adam Lehar[a], Renata Rydzik[b], Harshpreet Chandok[a], Yun-Sil Lee[c,d], Daniel W. Youngstrom[b], Joshy George[a], Martin M. Matzuk[e,f], Emily L. Germain-Lee[g,h,i], and Se-Jin Lee[a,j,1]

[a]The Jackson Laboratory for Genomic Medicine, Farmington, CT 06032; [b]Department of Orthopaedic Surgery, University of Connecticut School of Medicine, Farmington, CT 06030; [c]Department of Molecular Genetics, Seoul National University, Seoul 08826, Republic of Korea; [d]Dental Research Institute, School of Dentistry, Seoul National University, Seoul 08826, Republic of Korea; [e]Department of Pathology and Immunology, Baylor College of Medicine, Houston, TX 77030; [f]Center for Drug Discovery, Baylor College of Medicine, Houston, TX 77030; [g]Department of Pediatrics, University of Connecticut School of Medicine, Farmington, CT 06030; [h]Center for Regenerative Medicine and Skeletal Development, University of Connecticut School of Dental Medicine, Farmington, CT 06030; [i]Division of Endocrinology, Center for Rare Bone Disorders, Connecticut Children's, Farmington, CT 06032; and [j]Department of Genetics and Genome Sciences, University of Connecticut School of Medicine, Farmington, CT 06030

Contributed by Se-Jin Lee, July 8, 2021 (sent for review June 20, 2021; reviewed by Mark W. Hamrick and Kunihiro Tsuchida)

Skeletal muscle and bone homeostasis are regulated by members of the myostatin/GDF-11/activin branch of the transforming growth factor-β superfamily, which share many regulatory components, including inhibitory extracellular binding proteins and receptors that mediate signaling. Here, we present the results of genetic studies demonstrating a critical role for the binding protein follistatin (FST) in regulating both skeletal muscle and bone. Using an allelic series corresponding to varying expression levels of endogenous *Fst*, we show that FST acts in an exquisitely dose-dependent manner to regulate both muscle mass and bone density. Moreover, by employing a genetic strategy to target *Fst* expression only in the posterior (caudal) region of the animal, we show that the effects of *Fst* loss are mostly restricted to the posterior region, implying that locally produced FST plays a much more important role than circulating FST with respect to regulation of muscle and bone. Finally, we show that targeting receptors for these ligands specifically in osteoblasts leads to dramatic increases in bone mass, with trabecular bone volume fraction being increased by 12- to 13-fold and bone mineral density being increased by 8- to 9-fold in humeri, femurs, and lumbar vertebrae. These findings demonstrate that bone, like muscle, has an enormous inherent capacity for growth that is normally kept in check by this signaling system and suggest that the extent to which this regulatory mechanism may be used throughout the body to regulate tissue mass may be more significant than previously appreciated.

follistatin | myostatin | activin | bone mineral density | chalone

Myostatin (MSTN) is a transforming growth factor-β (TGF-β) superfamily member that normally acts to limit skeletal muscle mass (1). Mice lacking MSTN exhibit dramatic increases in skeletal muscle mass throughout the body, with individual muscles growing to about twice the normal size. The amino acid sequence of MSTN has been strongly conserved through evolution (2), and engineered or naturally occurring mutations in the *MSTN* gene have been shown to lead to increased muscling in many other species as well, including cattle (2–4), sheep (5), dogs (6), rabbits (7), rats (8), swine (9), goats (10), and humans (11). MSTN is regulated by various extracellular binding proteins, including follistatin (FST) (12), FSTL-3 (13), GASP-1 (14), and GASP-2 (15, 16), as well as the MSTN propeptide, which maintains MSTN in an inactive, latent state (12, 17–19). MSTN signals initially by binding to the activin type 2 receptors ACVR2 and ACVR2B (12, 20–22), followed by engagement of the type 1 receptors ALK4 and ALK5 (22, 23).

The function of MSTN as a negative regulator of muscle growth is partially redundant with that of another TGF-β family member, activin A (20, 24–27), which shares many regulatory and signaling components with MSTN. Indeed, one of these components, FST, was originally identified for its ability to inhibit secretion of follicle-stimulating hormone (FSH) by cultured pituitary cells (28), and subsequent work showed that FST is capable of binding and inhibiting activins (29), which are capable of signaling to pituitary gonadotrophs to induce FSH secretion (30). *FST* undergoes alternative splicing to generate two isoforms, the full-length FST315 and a carboxyl-terminal truncated FST288 (31). A third form, FST303, is derived from proteolytic cleavage of the C-terminal domain. All of the FST isoforms contain a heparin-binding domain that mediates binding to cell-surface proteoglycans. The presence of the C-terminal acidic tail in FST315, however, appears to neutralize the basic residues present in the heparin-binding domain and, as a result, FST315 binds poorly to proteoglycans and is the predominant form of FST in the circulation. FST288, which lacks the C-terminal 26–amino acid extension, tends to remain locally sequestered following secretion.

Based on the existence of these multiple isoforms and their differential biodistribution following secretion, a major question

Significance

Maintenance of skeletal muscle and bone is regulated by key signaling proteins belonging to the transforming growth factor family. Here, we present genetic studies in mice showing that follistatin, which normally blocks the activities of these proteins, acts locally in an exquisitely dose-dependent manner to control muscle and bone growth. Moreover, our studies targeting the receptors for these proteins reveal the enormous capacity for bone growth that is normally kept in check by this signaling system. These findings have implications for strategies to target this signaling pathway for clinical applications to treat patients with muscle and bone loss.

Author contributions: E.L.G.-L. and S.-J.L. conceptualized the project; Y.L. and S.-J.L. designed research; Y.L., A.L., R.R., H.C., Y.-S.L., and S.-J.L. performed research; M.M.M. contributed new reagents/analytic tools; Y.L., A.L., R.R., H.C., D.W.Y., J.G., E.L.G.-L., and S.-J.L. analyzed data; Y.L., E.L.G.-L., and S.-J.L. wrote the paper; and D.W.Y., J.G., E.L.G.-L., and S.-J.L. provided project administration.

Reviewers: M.W.H., Augusta University; and K.T., Fujita Ika Daigaku.

Competing interest statement: E.L.G.-L. and S.-J.L. are in the process of filing a patent application based on findings reported in this paper.

[1]To whom correspondence may be addressed. Email: sejlee@uchc.edu.

This article contains supporting information online at https://www.pnas.org/lookup/suppl/doi:10.1073/pnas.2111401118/-/DCSupplemental.

Published August 12, 2021.

has been whether the mode of action of FST is primarily local, regulating signaling by target ligands at or near the site of FST synthesis, or whether circulating FST can influence signaling to tissues distant from its site of synthesis. This question is relevant not only in terms of understanding the mechanism of action of FST but also in terms of interpreting human studies seeking associations between circulating FST levels and various physiological and pathological states. Here, we use genetic approaches in mice to address this fundamental question with respect to the roles of FST and this regulatory system in regulating two tissues, skeletal muscle and bone.

Results

A number of studies have shown that FST, by binding and inhibiting both MSTN and activin A, plays an important role in regulating muscle growth. Specifically, we showed that transgenic overexpression of FST in skeletal muscle leads to muscle hypertrophy, consistent with inhibition of the MSTN/activin A signaling pathway (12) and, conversely, that heterozygous loss of *Fst* in mice leads not only to reductions in muscle weights (by about 15 to 20%) but also to a shift toward oxidative fiber types, an impairment of muscle regeneration following cardiotoxin-induced injury, and reduced tetanic force production (25), all consistent with overactivity of this signaling pathway. $Fst^{-/-}$ mice have also been shown to have a reduced amount of muscle at birth (32), but because mice completely lacking FST are not viable, we sought to utilize mice carrying a conditional Fst^{flox} allele (33) to target *Fst* in specific cell types and regions of the body in order to examine the effects of FST loss in tissues of adult mice. Even after extensive backcrossing of the *flox* allele onto a C57BL/6 background, we noted that mice carrying this allele (in the absence of cre recombinase) were heavier than wild-type mice, with total body weights of $Fst^{flox/flox}$ mice being increased by 13 and 19% in males and females, respectively (*SI Appendix*, Table S1). These differences in body weights reflected increased expression of *Fst* from the *flox* allele (see below), likely resulting from retention of the neomycin selection cassette in the targeted locus during the construction of this mutant line (33).

The increased expression of *Fst* from the *flox* allele allowed us to generate mice carrying various combinations of wild-type, deletion, and *flox* alleles to produce an allelic series with varying levels of *Fst* expression. Analysis of the gastrocnemius muscle showed that we were able to generate *Fst* RNA expression levels ranging from a 30% decrease in $Fst^{+/-}$ mice to 55 and 82% increases in $Fst^{flox/+}$ and $Fst^{flox/flox}$ mice, respectively (Fig. 1*A*). Levels of circulating FST also generally followed the same trends, with serum FST levels being ∼50 and 200% of wild-type levels in $Fst^{+/-}$ and $Fst^{flox/flox}$ mice, respectively (Fig. 1*B*). These differences in *Fst* expression levels correlated not only with total body weight (*SI Appendix*, Table S1) but also with weights of individual muscles, which ranged from decreases of 18 to 23% in $Fst^{+/-}$ mice to increases of 29 to 48% in $Fst^{flox/flox}$ mice depending on the specific muscle and sex (Fig. 1 *A* and *C* and Table 1). $Fst^{flox/+}$ and $Fst^{flox/-}$ mice had intermediate muscle weights, reflecting intermediate *Fst* expression levels in these mice. Hence, FST acts in a dose-dependent manner to regulate muscle mass, with an approximately linear relationship between levels of FST expression and muscle weights.

Because $Fst^{-/-}$ mice die immediately after birth (32), we could not examine the effect of complete loss of FST in adult mice. To determine the effect of further loss of FST beyond that seen in $Fst^{+/-}$ mice, we examined the effect of targeting Fst^{flox} alleles in specific tissues and regions of the body. In one set of experiments, we examined the effect of targeting *Fst* in skeletal muscle using an *Myl1-cre* transgene (34), which we showed to be expressed specifically in myofibers but not in satellite cells (35). Male mice carrying one or more Fst^{flox} alleles in conjunction with *Myl1-cre* generally had lower circulating FST levels compared with mice lacking cre, demonstrating that myofiber-derived FST does contribute to the circulating pool (Fig. 1*B*); similar trends were seen in female mice, although the individual comparisons were not statistically significant. Targeting *Fst* in myofibers resulted in decreases in muscle weights in both males and females; although the effects were relatively small, many of the differences were statistically significant in both sexes (Fig. 1*C* and Table 1). Hence, myofiber-derived FST does play some role in regulating muscle mass.

Because the effects of targeting *Fst* in myofibers were small, however, we also examined the effects of more global targeting of *Fst* using the *Cdx2-cre* transgene, which is expressed specifically in the posterior (caudal) but not anterior (cranial) region of the animal (36); in particular, *Cdx2-cre* is expressed in all cells posterior to the umbilicus but not in any cells anterior to the umbilicus. In order to eliminate as much *Fst* expression as possible, we set up crosses of $Fst^{+/-}$; *Cdx2-cre* males with $Fst^{flox/flox}$ females and analyzed $Fst^{flox/-}$ offspring that were either negative or positive for *Cdx2-cre*. $Fst^{flox/-}$; *Cdx2-cre* mice were viable, which allowed us to analyze mice at adulthood. As shown in Table 1 and Fig. 1*D*, muscles located in the posterior region of $Fst^{flox/-}$; *Cdx2-cre* mice (quadriceps and gastrocnemius), where *Cdx2-cre* is expressed, exhibited significant decreases in muscle weights that exceeded those seen in $Fst^{+/-}$ mice (25) (see also Fig. 1*C*). These decreases were seen in both males and females and ranged from 51 to 58% in both muscle groups compared with $Fst^{flox/-}$ mice lacking *Cdx2-cre*.

To determine whether the decreased muscle sizes were due to differences in fiber numbers or fiber sizes, we carried out morphometric analysis of gastrocnemius muscles. Although we found no significant differences in fiber number between cre-negative and cre-positive muscles (*SI Appendix*, Table S2), myofiber sizes were significantly reduced in cre-positive muscles. As shown in Fig. 1*E*, the distribution of fiber sizes of $Fst^{flox/-}$; *Cdx2-cre* muscles had a similar overall shape to that of cre-negative mice but was shifted significantly to smaller diameters, with the mean fiber diameter being reduced from 45.4 μm in *Cdx2-cre*–negative mice to 33.6 μm in *Cdx2-cre*–positive mice. For comparison, we also carried out morphometric analysis of *F66* transgenic mice, which exhibit dramatic increases in muscle mass as a result of an *Myl1-Fst* transgene located on the Y chromosome (24). As we reported previously, fiber number in the gastrocnemius was increased by 12% in *F66* mice compared with wild-type mice (*SI Appendix*, Table S2), and the distribution of fiber diameters, which was slightly more spread out than in wild-type mice, was shifted to larger diameters, with mean fiber diameter being increased from 42.5 μm in wild-type mice to 59.7 μm in *F66* mice (Fig. 1*E*). Hence, by manipulating levels of *Fst* expression, we were able to generate an approximately fourfold range in muscle size, from a slightly over 50% decrease in $Fst^{flox/-}$; *Cdx2-cre* mice to an approximate doubling in *F66* mice.

Further histological examination of muscles from $Fst^{flox/-}$; *Cdx2-cre* mice revealed two other effects of FST loss. First, fiber type analysis of gastrocnemius muscles revealed a significant shift away from glycolytic type IIb fibers and toward mixed glycolytic/oxidative type IIa fibers and oxidative type I fibers in *Cdx2-cre*–positive muscles compared with cre-negative muscles (Fig. 2*A*). This fiber type shift is consistent with that seen in $Fst^{+/-}$ mice (25) but to a greater degree. In contrast, the reverse fiber type shift was seen in *F66* muscles compared with wild-type muscles; in fact, in *F66* gastrocnemius muscles, type I fibers were completely absent, and the percentage of type IIa fibers was reduced by nearly 50%. Hence, decreasing FST levels led to a fiber type shift toward more oxidative fibers, and increasing FST levels led to a fiber type shift toward more glycolytic fibers. Second, oil red O staining of gastrocnemius sections revealed the presence of numerous fat droplets in muscle fibers of $Fst^{flox/-}$; *Cdx2-cre* mice compared with cre-negative controls (Fig. 3*A*).

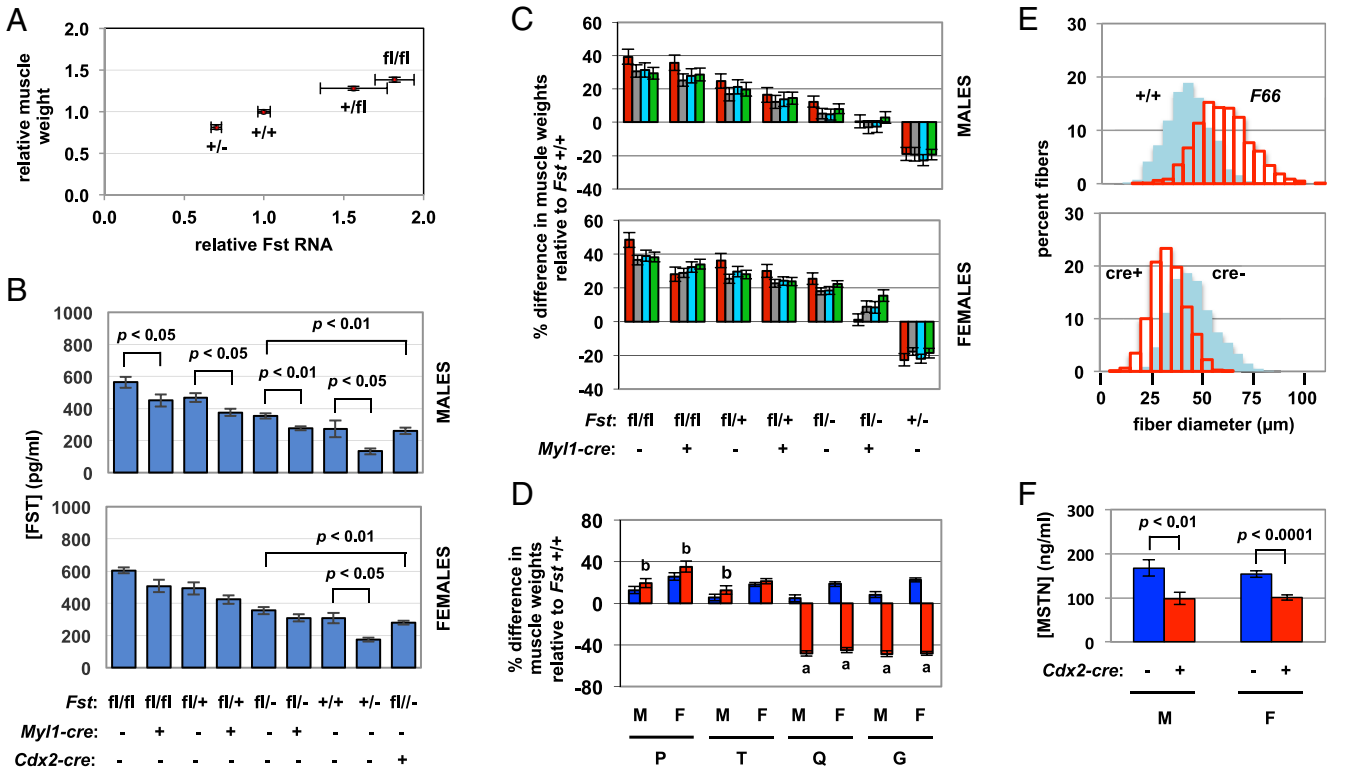

Fig. 1. Effect of *Fst* mutant alleles on skeletal muscle. (*A*) Weights of gastrocnemius muscles versus *Fst* RNA expression levels in mice carrying various combinations of *Fst* mutant alleles. Numbers are normalized to values for $Fst^{+/+}$ muscles. RNA expression levels were measured by qPCR ($n = 3$ mice per group), and muscle weights were taken from the data in Table 1. (*B*) Plasma FST levels in mice carrying various *Fst* mutant alleles with or without *Myl1-cre* or *Cdx2-cre* transgenes ($n = 4$ per group). (*C*) Relative weights of pectoralis (red), triceps (gray), quadriceps (blue), and gastrocnemius/plantaris (green) muscles in mice carrying various *Fst* mutant alleles with or without *Myl1-cre*. Numbers are expressed as percent increase/decrease relative to $Fst^{+/+}$ mice and were calculated from the data shown in Table 1. (*D*) Relative weights of muscles of $Fst^{fl/-}$ mice in the absence (blue bars) or presence (orange bars) of *Cdx2-cre*. Numbers are expressed as percent increase/decrease relative to $Fst^{+/+}$ mice and were calculated from the data shown in Table 1. G, gastrocnemius; P, pectoralis; Q, quadriceps; T, triceps. $^{a}P < 0.001$, $^{b}P < 0.05$ versus *Cdx2-cre*–negative mice. (*E*) Distribution of fiber sizes in gastrocnemius muscles of *F66* and $Fst^{+/+}$ mice (*Upper*) or $Fst^{fl/-}$; *Cdx2-cre*–negative and –positive mice (*Lower*). Fiber diameters were measured in muscles isolated from three mice (250 fibers per mouse) and pooled for plotting. (*F*) Plasma MSTN levels in $Fst^{fl/-}$; *Cdx2-cre*–negative and –positive mice ($n = 8$ per group). Error bars represent standard error of the mean (SEM). M, males; F, females.

These fat droplets were seen in the majority of muscle fibers and not just in type I and type IIa fibers, which have been reported to show lipid accumulation by histological examination (37). Quantification of representative sections by fluorescence imaging of Nile red–stained sections showed significantly increased fluorescence intensity in gastrocnemius muscles isolated from *Cdx2-cre*–positive compared with cre-negative mice (Fig. 3*B*). We also analyzed sections of muscles isolated from *F66* transgenic mice, which showed decreased fluorescence intensity compared with wild-type mice. Hence, the extent of fat accumulation in muscle was inversely correlated with levels of FST.

These histological changes with respect to fiber type shifts and lipid accumulation were consistent with changes in gene expression patterns in muscles isolated from these mice. RNA-sequencing (RNA-seq) analysis identified 399 up-regulated and 234 down-regulated transcripts in gastrocnemius muscles isolated from *Cdx2-cre*–positive compared with cre-negative mice (*SI Appendix*, Fig. S1). Among these differentially regulated genes were ones encoding myosin heavy-chain isoforms characteristic of specific fiber types (38, 39). In particular, *Myh7*, *Myh7B*, and *Myh2* were all up-regulated in *Cdx2-cre*–positive muscles, consistent with increased numbers of type I and type IIa fibers, and *Mhy4* was down-regulated, consistent with decreased numbers of type IIb fibers (Fig. 2*B*). We observed similar shifts in other sarcomere components as well (38, 39), including myosin light-chain, troponin, and tropomyosin isoforms, with components characteristic of slow fibers (*Myl2*, *Myl3*, *Myl6b*, *Myl10*, *Myl12a*, *Tnnc1*, *Tnni1*, *Tnnt1*, and *Tpm3*) being up-regulated and components characteristic of fast fibers (*Myl1*, *Mylpf*, *Tnnc2*, *Tnni2*, *Tnnt3*, and *Tpm1*) being down-regulated in *Cdx2-cre*–positive muscles. Moreover, expression levels of myosin light-chain kinase isoforms also tracked with these fiber type shifts, with *Mylk3* (slow fibers) and *Mylk2* (fast fibers) being up-regulated and down-regulated, respectively. Finally, we observed up-regulation of certain sarcomere protein isoforms not typically expressed in adult skeletal muscle, including *Myh8* (neonatal), *Myl4* (embryonic), *Tnnt2* (cardiac), and *Tpm2* (cardiac), raising the possibility that there might be enhanced regeneration occurring in *Cdx2-cre*–positive muscles. We did not, however, observe any increase in the number of centrally located nuclei in muscles of *Cdx2-cre*–positive mice. Also consistent with the histological changes were the results of pathway analysis of the entire set of differentially expressed transcripts in *Cdx2-cre*–positive muscles. Although no enriched pathways were identified among the 234 down-regulated transcripts, 25 enriched pathways were identified among the 399 up-regulated transcripts. Strikingly, of the 8 enriched pathways comprising the greatest number of genes, 7 corresponded to pathways involved in lipid metabolism (Fig. 3*C*). These pathways encompassed a total of 40 up-regulated genes, 36 of which encode enzymes directly involved in lipid metabolism (Table 2). Hence, changes in RNA

Table 1. Effect of the targeting *Fst* on muscle weights

	n	Pectoralis, mg	Triceps, mg	Quadriceps, mg	Gastrocnemius, mg
Males					
$Fst^{flox/flox}$	37	100.3 ± 1.8*	125.8 ± 2.1*	256.6 ± 3.9*	176.2 ± 2.3*
$Fst^{+/flox}$	17	89.8 ± 1.9*	112.4 ± 2.7*	236.8 ± 4.8*	163.0 ± 3.6*
$Fst^{flox/-}$	21	80.9 ± 1.1*	101.2 ± 1.7	204.5 ± 2.8	147.2 ± 1.5†
$Fst^{+/+}$	17	71.9 ± 2.0	96.1 ± 2.4	195.2 ± 5.7	136.1 ± 3.5
$Fst^{+/-}$	9	58.2 ± 2.3*	77.7 ± 3.3*	150.9 ± 4.7*	109.8 ± 3.3*
$Fst^{flox/flox}$ + *Myl1-cre*	20	97.7 ± 2.0	120.5 ± 1.8	249.8 ± 4.2	175.1 ± 2.7
$Fst^{+/flox}$ + *Myl1-cre*	17	83.8 ± 2.3‡	107.9 ± 2.6	222.1 ± 5.2‡	155.9 ± 3.1
$Fst^{flox/-}$ + *Myl1-cre*	8	72.4 ± 2.0§	93.3 ± 2.8‡	190.1 ± 4.2§	140.1 ± 3.2
$Fst^{flox/-}$ + *Cdx2-cre*	12	85.8 ± 1.6‡	108.3 ± 2.9‡	101.0 ± 3.7¶	70.0 ± 3.1¶
Females					
$Fst^{flox/flox}$	37	65.8 ± 1.2*	91.5 ± 1.4*	192.8 ± 3.3*	133.6 ± 2.2*
$Fst^{+/flox}$	25	60.4 ± 1.3*	84.1 ± 1.5*	179.8 ± 3.2*	123.6 ± 1.9*
$Fst^{flox/-}$	30	55.6 ± 0.9*	79.2 ± 1.0*	164.3 ± 1.7*	118.2 ± 1.2*
$Fst^{+/+}$	28	44.3 ± 1.0	67.1 ± 0.9	138.8 ± 2.3	96.6 ± 1.3
$Fst^{+/-}$	14	34.3 ± 1.4*	55.2 ± 1.3*	108.3 ± 3.2*	78.5 ± 2.5*
$Fst^{flox/flox}$ + *Myl1-cre*	22	56.7 ± 1.3¶	86.4 ± 1.4‡	183.5 ± 3.0‡	129.4 ± 2.1
$Fst^{+/flox}$ + *Myl1-cre*	21	57.6 ± 1.0	82.3 ± 1.2	172.2 ± 2.2	119.6 ± 1.8
$Fst^{flox/-}$ + *Myl1-cre*	14	44.8 ± 1.2¶	73.1 ± 2.0‡	150.3 ± 4.1§	111.5 ± 3.0‡
$Fst^{flox/-}$ + *Cdx2-cre*	10	59.9 ± 1.9‡	81.3 ± 1.5	76.4 ± 3.2¶	50.2 ± 1.8¶

*$P < 0.001$ vs. $Fst^{+/+}$.
†$P < 0.01$ vs. $Fst^{+/+}$.
‡$P < 0.05$ vs. cre^{-}.
§$P < 0.01$ vs. cre^{-}.
¶$P < 0.001$ vs. cre^{-}.

expression profiles in *Cdx2-cre*–positive muscles were consistent with changes that we observed on histological examination of the muscles.

A considerably larger number of differentially expressed genes were identified in RNA-seq analysis of *F66* muscles, with 2,274 up-regulated and 2,666 down-regulated transcripts compared with wild-type muscles (*SI Appendix*, Fig. S1). Among the down-regulated transcripts in *F66* muscles were 75 that were oppositely regulated (i.e., up-regulated) in *Cdx2-cre*–positive mice. Pathway analysis of this subset of 75 genes identified three enriched pathways, namely thermogenesis, the tricarboxylic acid (TCA) cycle, and oxidative phosphorylation. These three enriched pathways, which comprised overlapping sets of genes, included a total of 17 genes whose functions were consistent with the shift toward oxidative fibers seen in *Cdx2-cre*–positive mice and shift toward glycolytic fibers seen in *F66* mice (Table 3). Among the up-regulated transcripts in *F66* muscles were 101 that were oppositely regulated (i.e., down-regulated) in *Cdx2-cre*–positive mice. Pathway

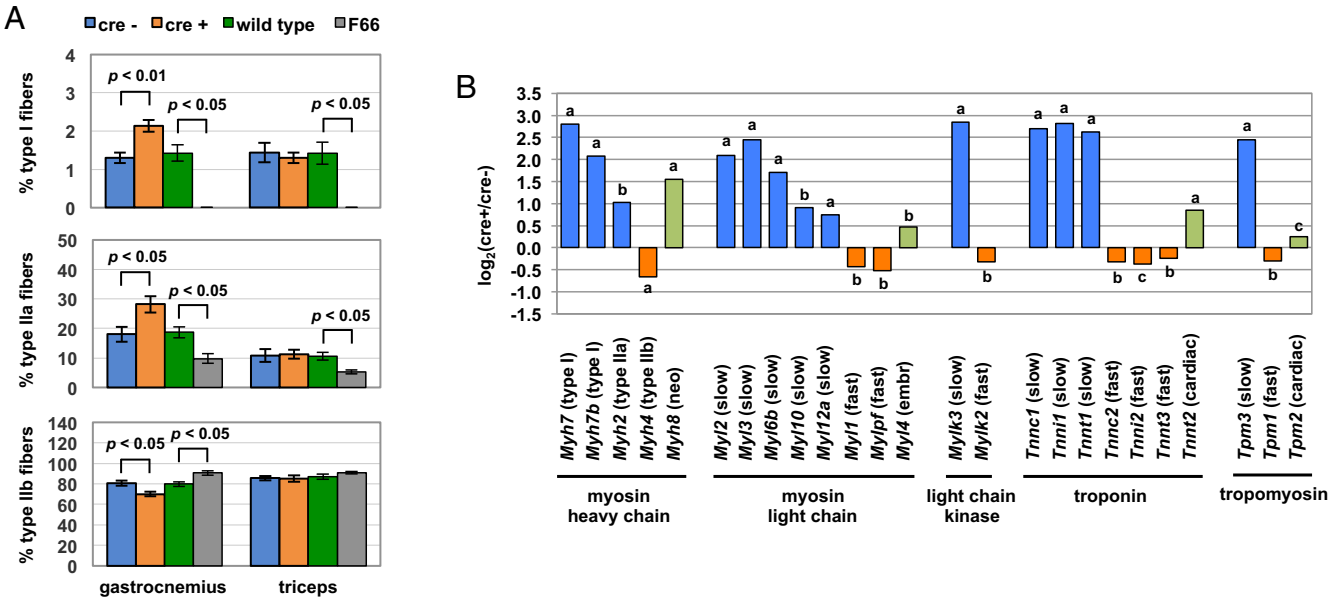

Fig. 2. Fiber type shifts in *Fst* mutant mice. (*A*) Percent type I, type IIa, and type IIb fibers in gastrocnemius and triceps muscles of $Fst^{fl/-}$; *Cdx2-cre* and *F66* mice ($n = 3$ per group). (*B*) Relative RNA expression levels for genes encoding sarcomeric protein isoforms and kinases. Numbers were determined by RNA-seq analysis and are presented as the $\log_2$ ratio of values obtained for *Cdx2-cre*–positive to *Cdx2-cre*–negative ($n = 9$ per group). Blue, slow isoforms; orange, fast isoforms; green, developmental and cardiac isoforms. Error bars represent SEM. $^{a}P < 0.001$, $^{b}P < 0.01$, $^{c}P < 0.05$.

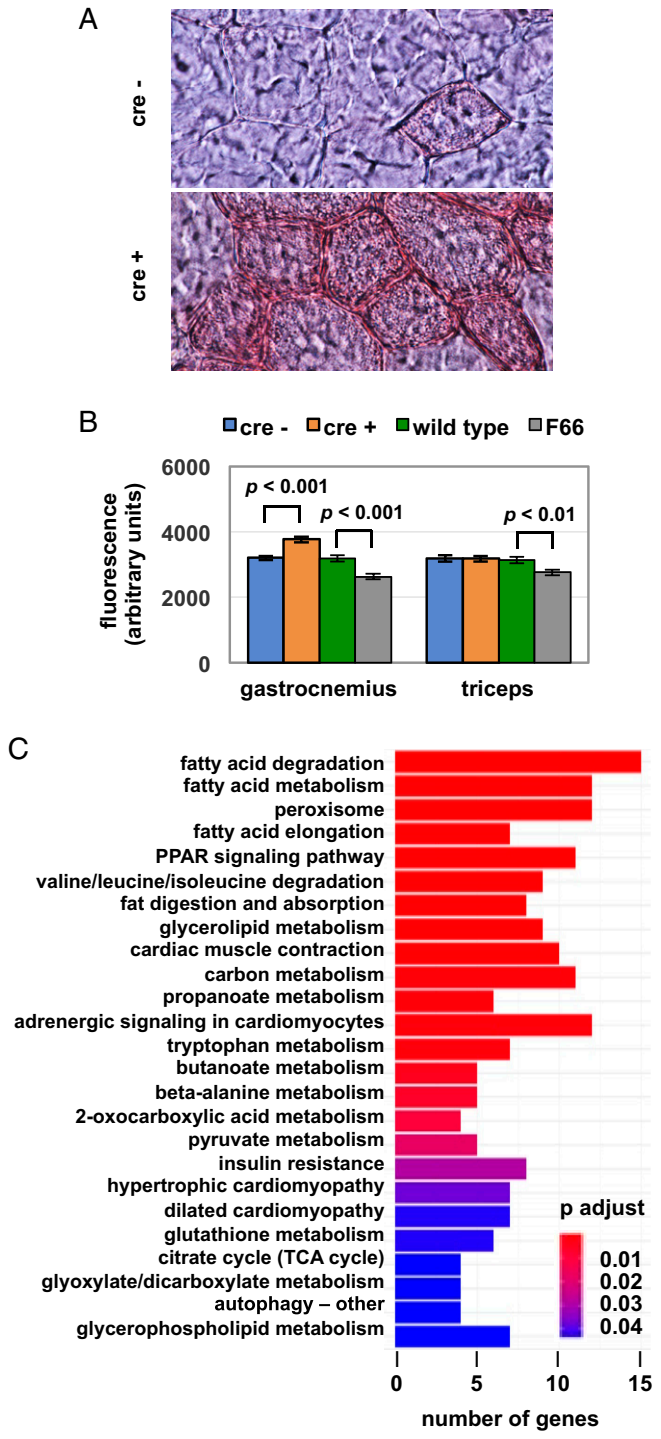

Fig. 3. Lipid accumulation in *Fst* mutant mice. (*A*) Oil red O stains of gastrocnemius sections of $Fst^{fl/-}$; *Cdx2-cre*–negative and –positive mice. (*B*) Fluorescence intensity of Nile red–stained sections of gastrocnemius and triceps muscles of $Fst^{fl/-}$; *Cdx2-cre* and *F66* mice. Numbers represent means of measurements taken from $Fst^{fl/-}$; *Cdx2-cre*–negative, $Fst^{fl/-}$; *Cdx2-cre*–positive, wild-type, and *F66* mice, with n = 5, 5, 7, and 7 mice, respectively, and with four representative sections analyzed for each mouse. (*C*) Up-regulated pathways identified by RNA-seq analysis of gastrocnemius muscles isolated from $Fst^{fl/-}$; *Cdx2-cre*–positive compared with cre–negative mice (n = 9 per group). Error bars represent SEM.

analysis of this subset of 101 genes identified seven enriched pathways, encompassing an overlapping set of 38 genes. Among these 38 genes were *Rps6kb1*, encoding ribosomal protein S6 kinase B1, which plays an important role in regulating protein synthesis, three protooncogenes (*Braf*, *Mras*, and *Nras*), and genes encoding 13 components of the cytoskeleton and extracellular matrix, including ankyrin 1, radixin, sarcoglycan alpha, decorin, thrombospondin 1, 2 integrin subunits, and 6 collagen chains (*SI Appendix*, Table S3).

The dramatic effects of FST loss seen in the quadriceps and gastrocnemius of $Fst^{flox/-}$; *Cdx2-cre* mice clearly show the important role that FST plays in regulating muscle size and structure. The effects seen in these mice could result either from loss of local action by FST or from loss of systemic action by FST, or both. Indeed, circulating levels of FST were decreased by 26 and 21% in $Fst^{flox/-}$; *Cdx2-cre* males and females, respectively (Fig. 1*B*), reflecting the fact that FST production is eliminated in the posterior region of the body in these mice. Given that the phenotype of $Fst^{flox/-}$; *Cdx2-cre* mice is much more pronounced than that seen in $Fst^{+/-}$ mice, which exhibit decreases in circulating FST levels by about 50%, and in $Fst^{flox/-}$; *Myl1-cre* mice, which exhibit decreases of slightly more than 20%, it seemed unlikely that systemic loss of FST could explain the greater effects seen in the quadriceps and gastrocnemius muscles of $Fst^{flox/-}$; *Cdx2-cre* mice compared with these other mice. To investigate further this question of local versus systemic modes of FST action, we analyzed muscles located in the anterior region of the animal where *Cdx2-cre* is not expressed. In contrast to the dramatic decreases in muscle weights seen in the posterior muscles, weights of anterior muscles (pectoralis and triceps) were not decreased in $Fst^{flox/-}$; *Cdx2-cre* mice (Fig. 1*D* and Table 1), implying that FST produced in the anterior region of the body is sufficient to maintain FST function in the anterior region even with the lower circulating levels of FST protein. Similarly, unlike the gastrocnemius, the triceps muscles showed no differences in fiber type distribution between *Cdx2-cre*–positive and cre-negative mice (Fig. 2*A*). Moreover, Nile red staining of triceps muscles showed no differences in fluorescence intensity between *Cdx2-cre*–positive and cre-negative mice, suggesting that the accumulation of fat droplets seemed to be restricted to the posterior region of the mice in which *Cdx2-cre* is expressed (Fig. 3*B*). Finally, whereas RNA-seq analysis of the gastrocnemius muscles identified a total of 633 differentially expressed transcripts between *Cdx2-cre*–positive and cre-negative mice, RNA-seq analysis of triceps muscles revealed no differences between *Cdx2-cre*–positive compared with cre-negative mice with an adjusted P value less than 0.05. In contrast, fiber type shifts toward glycolytic type IIb fibers and reductions in fat accumulation were seen in both the triceps and gastrocnemius muscles of *F66* mice (Figs. 2*A* and 3*B*), reflecting the fact that the *Fst*-overexpressing transgene was expressed in skeletal muscles throughout the body. The simplest interpretation of all these data is that FST acts predominantly, if not exclusively, in a local manner to regulate muscle size, fiber type, and lipid accumulation.

Analysis of the anterior muscles did reveal, however, some systemic effects of targeting *Fst* in the posterior region. In particular, instead of muscle weights being reduced in the anterior region of $Fst^{flox/-}$; *Cdx2-cre* mice, weights of the pectoralis and triceps muscles actually exhibited small but significant increases compared with cre-negative mice (Fig. 1*D* and Table 1), which is the opposite of what would be expected upon loss of FST. Although this effect on anterior muscles, which was seen in both males and females, could reflect a variety of physiological changes occurring in the animal as a result of loss of FST production in the posterior half of the body, we believe that a possible explanation is that circulating levels of MSTN in *Cdx2-cre*–positive mice are reduced by ~35 to 40% compared with cre-negative mice (Fig. 1*F*). Given that *Mstn* RNA levels were unchanged in both anterior and posterior muscles of *Cdx2-cre*–positive mice compared with

Table 2. Expression levels of genes identified in enriched pathways related to lipid metabolism that are up-regulated in *Cdx2-cre*–positive (relative to cre-negative) gastrocnemius muscles

Gene	Protein	Log_2 ratio	*P*
Acaa2	Acetyl-coA acyltransferase 2	+0.66	4.9E-7
Acadl	Acyl-coA dehydrogenase long chain	+0.73	4.4E-7
Acadm	Acyl-coA dehydrogenase medium chain	+0.76	7.6E-6
Acadvl	Acyl-coA dehydrogenase very long chain	+0.40	1.0E-3
Acat1	Acetyl-coA acetyltransferase 1	+0.46	9.2E-5
Acot1	Acyl-coA thioesterase 1	+0.47	1.2E-3
Acot2	Acyl-coA thioesterase 2	+0.91	1.4E-4
Acsl1	Acyl-coA synthetase long-chain family member 1	+0.79	3.3E-4
Agpat2	1-Acylglycerol-3-phosphate *O*-acyltransferase 2	+0.79	1.8E-3
Agpat3	1-Acylglycerol-3-phosphate *O*-acyltransferase 3	+0.36	3.8E-3
Aldh9a1	Aldehyde dehydrogenase 9 family member A1	+0.62	2.5E-4
Amacr	Alpha-methylacyl-coA racemase	+0.27	2.1E-3
Cat	Catalase	+0.46	3.3E-3
Cd36	Cluster of differentiation 36 (fatty acid translocase)	+0.69	1.0E-6
Cpt1b	Carnitine palmitoyltransferase 1B	+0.31	1.3E-3
Cpt2	Carnitine palmitoyltransferase 2	+0.35	7.5E-6
Dgat2	Diacylglycerol *O*-acyltransferase 2	+1.21	2.4E-5
Dhrs4	Dehydrogenase/reductase 4	+0.83	3.7E-7
Ech1	Delta(3,5)-delta(2,4)-dienoyl-coA isomerase	+0.54	5.6E-6
Echs1	Enyl-coA hydratase, short chain 1	+0.56	7.7E-5
Eci1	Enol-coA delta isomerase 1	+0.46	2.5E-4
Eci2	Enol-coA delta isomerase 2	+0.40	7.5E-7
Ephx2	Epoxide hydrolase 2	+0.75	1.8E-7
Fabp3	Fatty acid–binding protein 3	+1.15	3.7E-8
Gk	Glycerol kinase	+0.66	1.8E-3
Hadh	3-Hydroxyacyl-coA dehydrogenase	+0.72	6.2E-5
Hadha	Hydroxyacyl-coA dehydrogenase trifunctional multienzyme complex subunit alpha	+0.70	4.5E-4
Hadhb	Hydroxyacyl-coA dehydrogenase trifunctional multienzyme complex subunit beta	+0.72	6.2E-5
Idh2	Isocitrate dehydrogenase [NADP(+)] 2	+1.23	6.7E-9
Lpl	Lipoprotein lipase	+1.03	1.8E-7
Mlycd	Malonyl-coA decarboxylase	+0.52	4.9E-4
Nudt7	Peroxisomal coenzyme A diphosphatase	+0.56	3.7E-6
Pex6	Peroxisomal biogenesis factor 6	+0.42	2.2E-4
Phyh	Phytanoyl-coA 2-hydroxylase	+0.35	8.0E-4
Pla2g12a	Phospholipase A2 group XIIA	+0.89	2.9E-9
Plin5	Perilipin-5	+1.44	6.7E-8
Plpp1	Phospholipid phosphatase 1	+0.27	5.9E-4
Plpp2	Phospholipid phosphatase 2	+0.87	1.8E-3
Pnpla2	Patatin-like phospholipase domain-containing 2	+0.45	6.4E-5
Slc27a1	Solute carrier family 27 member 1 (long-chain fatty acid transport protein 1)	+0.72	7.2E-6

cre-negative mice (*SI Appendix*, Fig. S2), the drop in circulating MSTN levels likely reflects the reduced amount of total muscle mass in $Fst^{flox/-}$; *Cdx2-cre* mice. We have shown that skeletal muscle is by far the predominant source of circulating MSTN protein (22) and, in a previous study using a similar approach to target an $Mstn^{flox}$ allele in the posterior region of the body with *Cdx2-cre*, we showed that MSTN acts to regulate muscle mass both by autocrine/paracrine and by endocrine modes of signaling (40). Hence, the reduction in circulating MSTN in $Fst^{flox/-}$; *Cdx2-cre* mice would be predicted to compensate partially for reduced FST with respect to control of muscle mass and, in anteriorly located muscles, lower circulating MSTN levels would be expected to cause increases in muscle growth.

In addition to the key role that the MSTN/activin A signaling pathway plays in regulating muscle mass, several studies have shown that this regulatory system is also important in the regulation of bone structure and bone density. Specifically, systemic administration of a decoy receptor consisting of the extracellular domain of ACVR2B fused to an immunoglobulin Fc domain has been shown to cause significant increases in bone mineral density and various microcomputed tomography (micro-CT) parameters, such as bone volume/total volume (BV/TV), connectivity density, and trabecular number (41–45), which are also seen to a milder degree upon targeting *Acvr2* and *Acvr2b* specifically in osteoblasts in vivo (44). Given that FST is capable of blocking the activities of ligands signaling through activin type 2 receptors, we investigated the effects of manipulating *Fst* expression levels on bone density and structure. As shown in *SI Appendix*, Tables S4–S8 and Fig. 4 *A* and *B*, micro-CT analysis of femurs, humeri, and L4 and L5 vertebrae showed opposite trends in $Fst^{flox/flox}$ and $Fst^{+/-}$ mice in comparison with wild-type mice. Specifically, parameters such as bone volume, bone surface, BV/TV, connectivity density, trabecular number, trabecular thickness, and bone mineral density were generally higher in bones of $Fst^{flox/flox}$ mice and were generally lower in bones of $Fst^{+/-}$ mice compared with those of wild-type mice. Many, though not all, of the differences

Table 3. Expression levels of genes identified in enriched pathways that are both up-regulated in *Cdx2-cre*–positive (relative to cre-negative) and down-regulated in *F66* (relative to wild-type) gastrocnemius muscles

Gene	Protein	*Cdx2-cre* $\log_2$ ratio	*P*	*F66* $\log_2$ ratio	*P*
Adcy6	Adenylate cyclase 6	+0.25	1.7E-2	−0.48	1.6E-5
Atp5b	ATP synthase F1 subunit beta	+0.22	2.1E-2	−0.21	3.2E-2
Atp5c1	ATP synthase F1 subunit gamma	+0.16	9.3E-3	−0.30	3.9E-6
Atp5pb	ATP synthase peripheral stalk-membrane subunit B	+0.28	5.3E-4	−0.22	6.2E-3
Coa4	Cytochrome *C* oxidase assembly factor 4 homolog	+0.45	4.9E-3	−0.36	4.1E-2
Cox5a	Cytochrome *C* oxidase subunit 5A	+0.33	1.5E-2	−0.36	8.6E-3
Cox7a2l	Cytochrome *C* oxidase subunit 7A2-like	+0.32	2.5E-6	−0.16	1.8E-2
Idh3b	Isocitrate dehydrogenase [NAD(+)] 3 noncatalytic subunit beta	+0.29	1.2E-3	−0.23	9.8E-3
Idh3g	Isocitrate dehydrogenase [NAD(+)] 3 noncatalytic subunit gamma	+0.16	1.1E-2	−0.37	4.6E-8
Lipe	Lipase E, hormone sensitive type	+0.38	2.2E-2	−1.10	4.2E-9
Mdh2	Malate dehydrogenase 2	+0.15	3.2E-2	−0.24	1.2E-3
Ndufaf4	NADH-ubiquinone oxidoreductase complex assembly factor-4	+0.18	3.2E-2	−0.32	3.0E-4
Ndufv1	NADH-ubiquinone oxidoreductase core subunit V1	+0.26	1.7E-2	−0.24	2.6E-2
Pdhb	Pyruvate dehydrogenase E1 subunit beta	+0.27	2.5E-3	−0.19	3.1E-2
Prkag1	Protein kinase AMP-activated noncatalytic subunit gamma-1	+0.22	2.5E-3	−0.28	1.8E-4
Sdhc	Succinate dehydrogenase complex subunit C	+0.30	4.7E-3	−0.30	4.8E-3
Uqcrc1	Ubiquinol-cytochrome *C* reductase core protein 1	+0.19	3.4E-2	−0.24	1.1E-2

These genes were identified as corresponding to enriched pathways for thermogenesis, the TCA cycle, and oxidative phosphorylation.

observed among the different genotypes were statistically significant, and the general trends were clearly evident in considering data from both males and females as well as from multiple bones. Hence, as in the case of muscle mass, varying levels of *Fst* expression also affected bone structure, with reduced levels of *Fst* expression leading to reduced bone density, demonstrating that FST plays an important, dose-dependent role in regulating bone homeostasis.

To determine whether FST acts locally versus systemically to regulate bone density, we analyzed the bones of $Fst^{flox/-}$; *Cdx2-cre* mice. We first carried out dual-energy X-ray absorptiometer (DXA) analysis in which we compared different regions of the body in *Cdx2-cre*–positive versus cre-negative mice. As shown in *SI Appendix*, Table S9, bone density by DXA was significantly lower in *Cdx2-cre*–positive compared with cre-negative mice in examining bones located in the posterior region of the body, including left and right femurs as well as L2/L3 and L4/L5 vertebrae. In contrast, bone density in either the left or right humerus was similar between *Cdx2-cre*–positive and cre-negative mice. Hence, bone density appeared to be affected in bones located in the posterior but not anterior region of the body. To examine bone structure in greater detail, we carried out micro-CT analysis of various bones isolated from these mice. Analysis of femurs showed that bone volume, bone surface, BV/TV, connectivity density, trabecular number, trabecular thickness, and bone mineral density were all significantly reduced in *Cdx2-cre*–positive compared with cre-negative mice (Fig. 4*C* and *SI Appendix*, Tables S10 and S11). These decreases were not seen, however, in micro-CT analysis of humeri isolated from these mice, and some of these parameters, such as bone volume, bone surface, BV/TV, and connectivity density, were even slightly increased in *Cdx2-cre*–positive compared with cre-negative male mice. Although we do not understand the basis for these small increases, the fact that decreases in bone density were seen in femurs but not in humeri of *Cdx2-cre*–positive mice suggests that FST acts locally to regulate bone structure.

The effects on bone seen upon manipulating expression levels of *Fst* are consistent with prior studies showing that pharmacological inhibition of signaling by systemic administration of the ACVR2B/Fc decoy receptor can cause dramatic changes in bone structure, including increases in bone density, BV/TV, connectivity density, and trabecular number and thickness (41–45). Moreover, targeting *Acvr2* either alone or in combination with *Acvr2b* in osteoblasts in vivo also leads to increases in femoral BV/TV and trabecular number (44). The effects of targeting *Acvr2* and *Acvr2b* in osteoblasts, however, were milder than those seen following treatment with ACVR2B/Fc, and treatment with ACVR2B/Fc was shown to cause even further increases in these parameters in mice in which both receptors were targeted in osteoblasts. These findings imply either that targeting the two activin type 2 receptors ACVR2 and ACVR2B may not be sufficient to completely block signaling by key ligands to osteoblasts or that osteoblasts may not be the sole target for these ligands with respect to regulation of bone homeostasis. To address the former possibility, we examined the effect of targeting ALK4 and ALK5, which are the two type 1 receptors utilized by MSTN and activin A in regulating skeletal muscle mass (22). Specifically, we used mice carrying floxed alleles for *Alk4* and *Alk5* to examine the effect of simultaneously targeting these type 1 receptors utilizing the osteocalcin-cre (*Oc-cre*) transgene, which has been shown to be expressed specifically in osteoblasts (46). For comparison, we also analyzed mice in which we simultaneously targeted *Acvr2* and *Acvr2b* using the same *Oc-cre* transgene.

By micro-CT analysis, very few differences were detected in femurs, humeri, or L5 vertebrae of $Acvr2^{flox/flox}$; $Acvr2b^{flox/flox}$; *Oc-cre* mice compared with cre-negative mice in either males or females (Fig. 5*A* and *SI Appendix*, Tables S12–S14). In contrast, the effects on bone structure in $Alk4^{flox/flox}$; $Alk5^{flox/flox}$; *Oc-cre* mice were readily apparent upon visual inspection of the micro-CT images (Fig. 5*B*), and nearly all of the micro-CT parameters showed dramatic differences compared with cre-negative control mice in all of the bone groups analyzed in both males and females (Fig. 5*A* and *SI Appendix*, Tables S12–S14). In females, for example, BV/TV was increased by 12- to 13-fold and bone mineral density was increased by 8- to 9-fold in humeri, femurs, and L5 vertebrae of $Alk4^{flox/flox}$; $Alk5^{flox/flox}$; *Oc-cre* mice compared with cre-negative mice. Hence, targeting signaling specifically in osteoblasts leads to massive increases in bone volume and density, with the effects of targeting the two type 1 receptors being much more pronounced compared with targeting the two type 2 receptors.

Finally, we carried out genetic studies investigating whether MSTN and activin A are the key ligands signaling through ALK4 and ALK5 to regulate bone. Previous studies have shown that bones of $Mstn^{-/-}$ mice have altered morphology and increased density (for a review, see ref. 47), suggesting that MSTN plays either a direct or indirect role in regulating bone structure. The

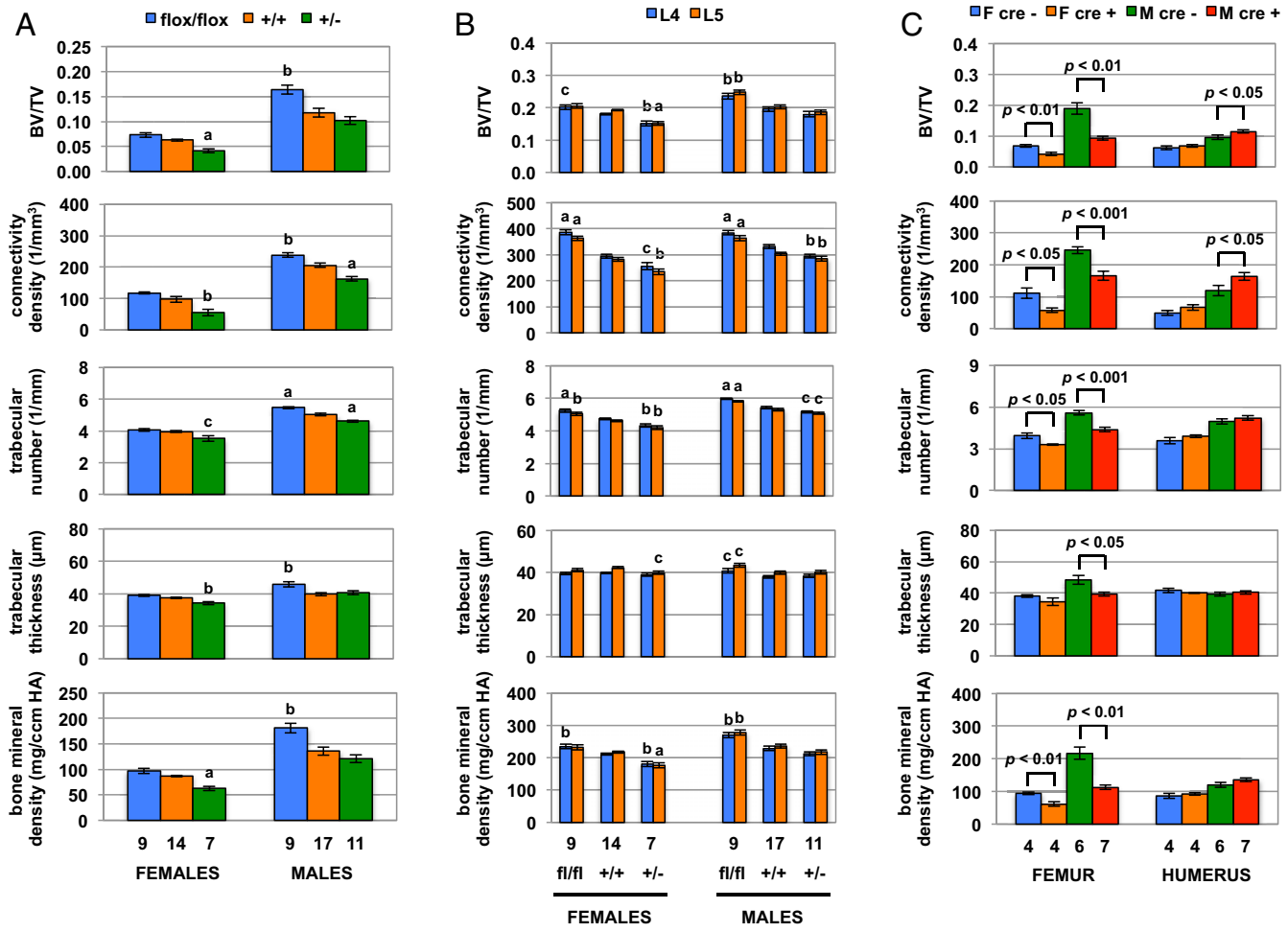

Fig. 4. Effect of *Fst* mutant alleles on bone. (*A* and *B*) Micro-CT analysis of (*A*) femurs and (*B*) L4 and L5 vertebrae of $Fst^{flox/flox}$, $Fst^{+/+}$, and $Fst^{+/-}$ mice. $^{a}P < 0.001$, $^{b}P < 0.01$, $^{c}P < 0.05$. (*C*) Micro-CT analysis of femurs and humeri isolated from $Fst^{fl/-}$; *Cdx2-cre*–negative and –positive mice. Numbers of mice per group are shown below. Error bars represent SEM.

effects of *Mstn* loss on parameters such as bone density, however, have been reported to be relatively mild compared with the effects that we have observed targeting the type 1 receptors in osteoblasts. Therefore, we examined the effect of loss of *Inhba* (encoding the βA-subunit of activin A and activin AB) on bone structure. Because complete loss of *Inhba* leads to embryonic lethality (48), we examined the effect of targeting *Inhba* in a regionally restricted manner using the *Cdx2-cre* transgene by targeting an $Inhba^{flox}$ allele only in the posterior region of the animal. In order to maximize the potential effects on bone, we simultaneously targeted *Mstn* using an $Mstn^{flox}$ allele in conjunction with the *Cdx2-cre* transgene.

By DXA analysis, lean body mass was significantly increased in $Mstn^{flox/flox}$; $Inhba^{flox/flox}$; *Cdx2-cre* mice compared with that of cre-negative mice, which could be attributed almost entirely to increases in the posterior half of the animals (Fig. 6*A*). Analysis of individual muscles revealed that weights of the quadriceps and gastrocnemius muscles were increased by 111 and 185%, respectively, compared with cre-negative mice (Fig. 6*B*). In a previous study, we showed that targeting *Mstn* alone in the posterior half of the animal using this same approach led to increases in weights of the quadriceps and gastrocnemius muscles by 73 and 85%, respectively (40). Hence, targeting *Mstn* and *Inhba* together led to much more substantial increases in muscle mass compared with targeting *Mstn* alone, consistent with prior studies documenting that activin A is capable of cooperating with MSTN to limit muscle growth (20, 24–27). Targeting *Mstn* and *Inhba* also led to significant changes in bone structure. As in the case of muscle, by DXA analysis, bone mineral density was increased in the posterior half of $Mstn^{flox/flox}$; $Inhba^{flox/flox}$; *Cdx2-cre* mice (Fig. 6*A*). By micro-CT analysis, parameters such as BV/TV, trabecular number, and bone mineral density were all significantly increased in femurs of $Mstn^{flox/flox}$; $Inhba^{flox/flox}$; *Cdx2-cre* mice (Fig. 6*C*); the effects, however, were significantly milder than those seen upon targeting *Alk4* and *Alk5*.

To determine whether these ligands act in an autocrine/paracrine or endocrine manner to regulate muscle and bone, we analyzed tissues isolated from the anterior region of $Mstn^{flox/flox}$; $Inhba^{flox/flox}$; *Cdx2-cre* mice. We previously showed that targeting *Mstn* in the posterior region leads not only to significant increases in weights of posteriorly located muscles but also to modest increases in weights of anteriorly located muscles (40). As shown in Fig. 6*B*, weights of pectoralis and triceps muscles, which are located in the anterior region, were increased by ∼25% in $Mstn^{flox/flox}$; $Inhba^{flox/flox}$; *Cdx2-cre* mice compared with cre-negative mice, consistent with a systemic role of circulating MSTN and/or activin A in regulation of muscle mass. In contrast, although we observed trends toward increased BV/TV, trabecular number, and bone mineral density in humeri of male mice (Fig. 6*C*), none of these differences were significant, and these parameters trended in the opposite direction in female mice. Hence,

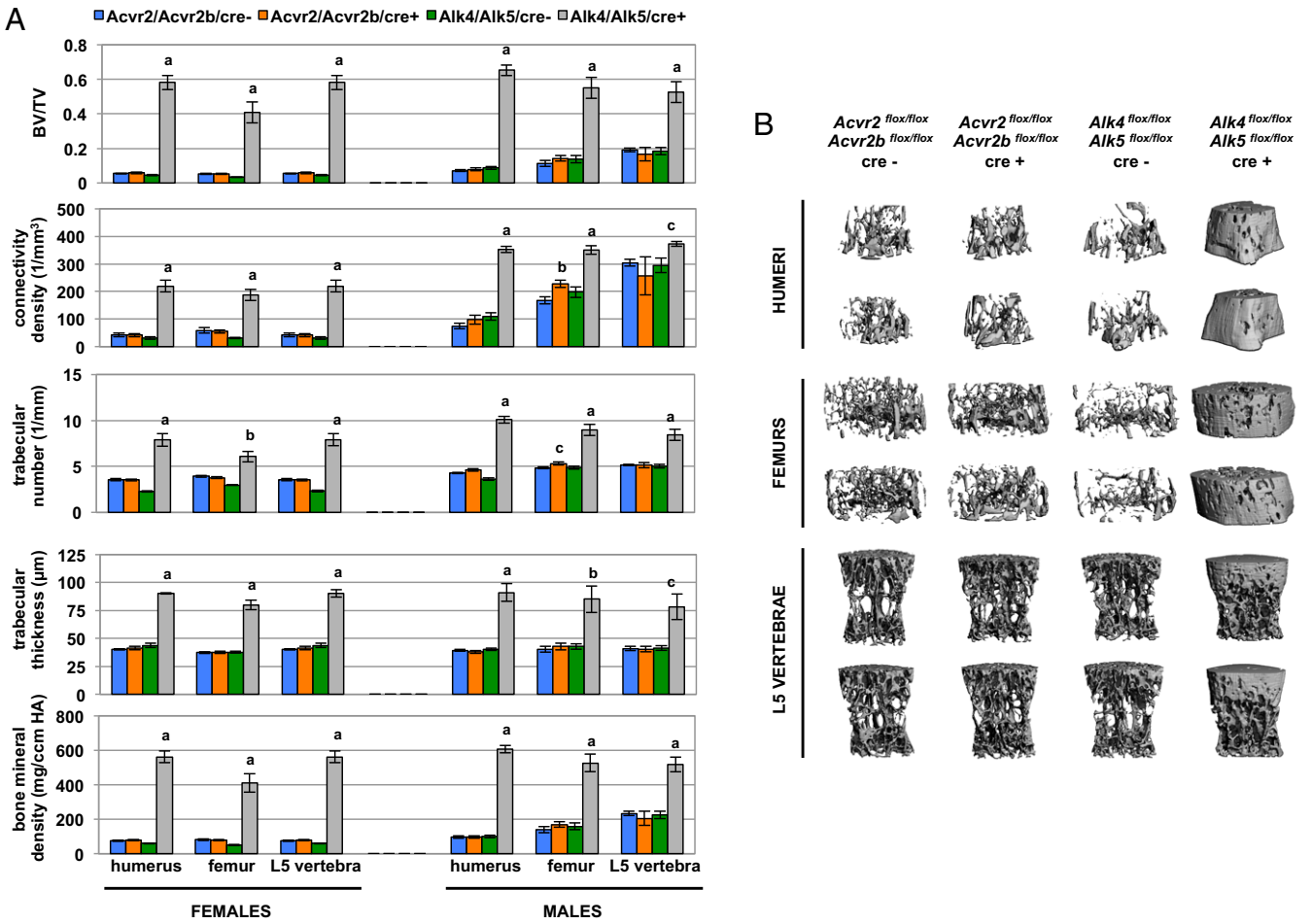

Fig. 5. Effect of targeting type 2 and type 1 receptors in osteoblasts. (*A*) Micro-CT analysis of humeri, femurs, and L5 vertebrae of $Acvr2^{flox/flox}$; $Acvr2b^{flox/flox}$; *Oc-cre*–negative ($n = 9$ females and 9 males), $Acvr2^{flox/flox}$; $Acvr2b^{flox/flox}$; *Oc-cre*–positive ($n = 9$ females and 6 males), $Alk4^{flox/flox}$; $Alk5^{flox/flox}$; *Oc-cre*–negative ($n = 6$ females and 9 males), and $Alk4^{flox/flox}$; $Alk5^{flox/flox}$; *Oc-cre*–positive ($n = 6$ females and 7 males) mice. $^{a}P < 0.001$, $^{b}P < 0.01$, $^{c}P < 0.05$. (*B*) Representative micro-CT images. Error bars represent SEM.

these ligands appear to act predominantly locally to regulate bone structure.

Discussion

Here, we present the results of genetic studies demonstrating a critical role for FST in regulating both skeletal muscle and bone homeostasis. Using an allelic series corresponding to varying *Fst* RNA expression levels and circulating FST protein levels, we show that FST acts in an exquisitely dose-dependent manner to regulate both muscle mass and bone density. With respect to muscle, reductions in FST levels lead not only to decreased muscle mass but also a shift toward oxidative fibers and increased intramuscular lipid accumulation, and, conversely, increased FST levels lead to increased muscle mass, a shift toward glycolytic fibers, and reduced lipid accumulation. With respect to bone, altered levels of FST lead to significant changes in bone structure, with reductions in FST levels leading to decreased bone density, decreased BV/TV, decreased trabecular number, and decreased trabecular thickness. Moreover, by employing a genetic strategy to target *Fst* expression only in the posterior region of the animal, we show that the effects of Fst loss are mostly restricted to the posterior region, implying that FST acts predominantly in a local manner in both muscle and bone. Our findings suggest that locally produced FST, most likely the FST288 isoform, plays a much more important role than circulating FST, at least with respect to regulation of muscle and bone. In the case of muscle, our results targeting *Fst* in myofibers suggest that although myofiber-derived FST does play a role in the overall regulation of muscle mass, FST derived from other cell types plays a more substantial role. Additional studies will be required to identify the key sources of FST for both muscle and bone, and our studies suggest that these sources must be local to these tissues. We believe that these findings have important implications both with respect to understanding the physiological mechanisms by which muscle and bone homeostasis are regulated by members of the TGF-β family and with respect to the interpretation of studies attempting to correlate circulating levels of FST with various disease states in humans.

Given that the only known mode of action of FST is to bind to and inhibit the activities of members of the TGF-β family of secreted signaling molecules, the effects of altered levels of FST seen in our studies almost certainly reflect altered levels of signaling by various TGF-β family members that are normally targets for FST. Previous studies have demonstrated that blocking the activities of certain TGF-β ligands using a decoy form of the ACVR2B/Fc receptor can lead to dramatic increases in muscle mass (20) and bone density (41–45), implying that the key ligands involved in regulating muscle and bone are likely to be ones capable of binding both FST and ACVR2B/Fc. Two such ligands are MSTN and activin A, and extensive genetic and pharmacological studies have documented the critical role that MSTN and activin A play in regulating muscle growth (1, 20, 24–27). Here, we present definitive genetic studies showing that targeting these

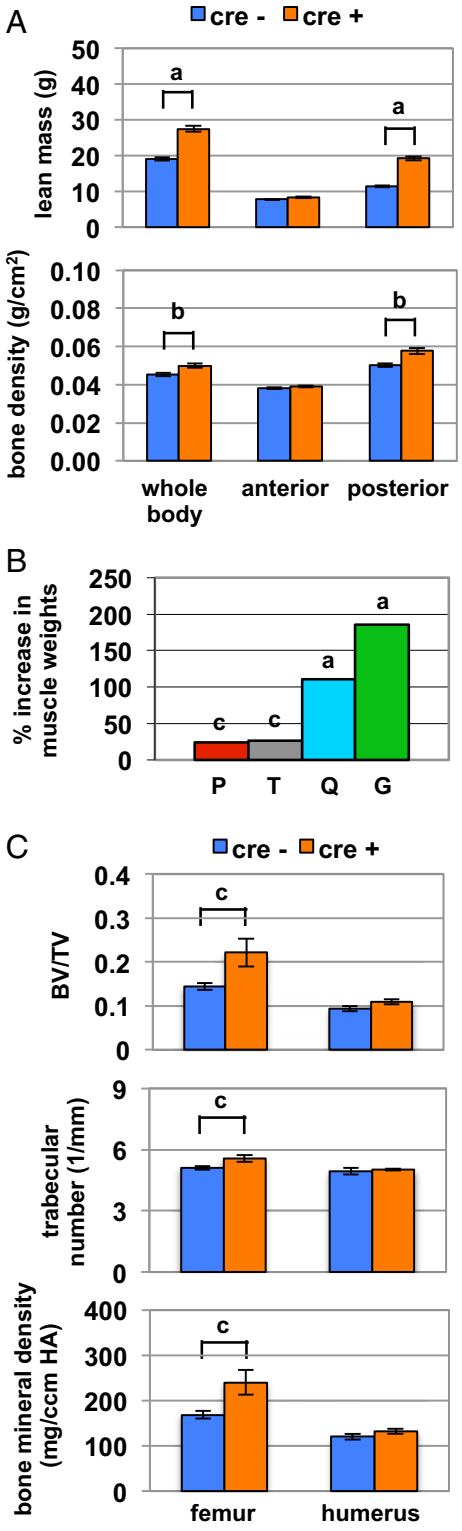

Fig. 6. Effect of targeting *Mstn* and *Inhba* in the posterior half of mice. (*A*) Lean body mass (*Upper*) and bone mineral density (*Lower*) of *Mstn*$^{flox/flox}$; *Inhba*$^{flox/flox}$; *Cdx2-cre*–negative (n = 8) and –positive (n = 8) mice by DXA analysis. Data are shown for the whole body or just the anterior or posterior half of the body. (*B*) Muscle weight increases in *Mstn*$^{flox/flox}$; *Inhba*$^{flox/flox}$; *Cdx2-cre* mice relative to cre-negative control mice. P, pectoralis; T, triceps; Q, quadriceps; G, gastrocnemius. (*C*) Micro-CT analysis of humeri and femurs of *Mstn*$^{flox/flox}$; *Inhba*$^{flox/flox}$; *Cdx2-cre*. Error bars represent SEM. $^{a}P < 0.001$, $^{b}P < 0.01$, $^{c}P < 0.05$.

two ligands simultaneously can lead to massive muscle growth. Furthermore, by targeting these ligands only in the posterior region of mice, we observed systemic effects in terms of muscle mass increases in anteriorly located muscles. These findings taken together with results of similar studies in which we targeted *Mstn* alone in the posterior region (40) demonstrate that MSTN and activin A each act in both an autocrine/paracrine and an endocrine manner to regulate muscle mass. In this regard, we observed that targeting *Fst* only in the posterior region led to reduced mass of posteriorly located muscles but actually had the reverse effect of slightly increasing mass of anteriorly located muscles, which is the opposite of what would be predicted for increased signaling by MSTN and/or activin A. We believe that this effect in anterior muscles is most likely the result of the dramatically reduced muscle mass in the posterior region of *Fst*$^{flox/-}$; *Cdx2-cre* mice leading to decreased circulating levels of MSTN, which through its endocrine mode of action then affects muscles throughout the body. In contrast to muscle, less is known regarding the key ligands being targeted by FST and ACVR2B/Fc in bone, as definitive genetic studies examining the effects of targeting this subgroup of ligands in bone have not yet been reported. Here, we show that targeting MSTN and activin A leads not only to increases in muscle mass but also to increases in bone density. Although the effects of targeting these two ligands were significant, the magnitude of the effects was considerably lower than what we were able to achieve by targeting the receptors for these ligands, implying that other ligands utilizing these receptors must also play important roles in regulating bone homeostasis. Moreover, unlike in the case of muscle, we were unable to detect systemic effects on bone from targeting these ligands in a regionally restricted manner, suggesting that these ligands act predominantly locally to regulate bone density.

Whatever the key ligands may be in bone, targeting signaling in osteoblasts is sufficient to cause changes in bone structure, including increases in bone mass and density, demonstrating that osteoblasts are direct targets for signaling by these ligands in vivo. It is also possible that changes in muscle mass in some of these studies could also indirectly affect bone structure, for example as a result of changes in mechanical forces exerted by the muscles or changes in release of myokines that signal to bone. In a previous study, we showed that by targeting *Acvr2* and *Acvr2b* in myofibers, we were able to increase muscle mass by 40 to 70% without observing any changes in bone structure by micro-CT analysis (22), suggesting that most, if not all, of the changes that we observed in bone structure described here as a result of pathway inhibition likely reflect modulation of signaling by ligands directly to bone. It is certainly possible, however, that indirect effects from reduced muscle mass in *Fst*-targeted mice may secondarily affect bone by either mechanism. Although we observed minimal effects of targeting the two type 2 receptors, ACVR2 and ACVR2B, in osteoblasts, the effects on bone structure and density were extensive upon targeting the two type 1 receptors, ALK4 and ALK5. The increases in parameters such as BV/TV and bone mineral density seen upon targeting ALK4 and ALK5 were quite remarkable, reaching levels of 12- to 13-fold in the case of BV/TV and 8- to 9-fold in the case of bone mineral density. We previously reported a similar discrepancy in the magnitude of muscle mass increases resulting from targeting these receptors in myofibers (22). In particular, we observed significant increases in muscle mass upon targeting ACVR2 and ACVR2B but substantially greater increases in muscle mass (up to threefold) upon targeting ALK4 and ALK5. The differential effects observed upon targeting type 1 versus type 2 receptors in both bone and muscle suggest that the simple model that combinations of ACVR2 and ACVR2B with ALK4 and ALK5 mediate all of the signaling by key TGF-β–related ligands in these tissues is likely incomplete. One possible explanation could be that this model is missing a key type 2 receptor or that signaling can occur through

some other mechanism. An alternative explanation could be that the spectrum of ligands being blocked by targeting ACVR2 and ACVR2B may be different from those being blocked by targeting ALK4 and ALK5. For example, TGF-β is also known to signal through ALK5, but TGF-β utilizes a different type 2 receptor, namely TGFBR2, to couple to ALK5, raising the possibility that loss of TGF-β signaling may have contributed to the effects seen upon targeting ALK5. Similarly, it is known that certain BMPs are capable of utilizing activin type 2 receptors for signaling, and BMP signaling has been shown to have the opposite effect of MSTN/activin A signaling in both muscle (49, 50) and bone (for a review, see ref. 51). Hence, it is possible that reduced levels of BMP signaling may have partially compensated for loss of MSTN/activin A signaling resulting from targeting *Acvr2* and *Acvr2b* in muscle and/or bone. In this regard, it is possible that levels of BMP activity may also have been affected in mice with altered FST levels, as FST is capable of binding and inhibiting BMPs as well.

Further study of this regulatory system will be critical not only for understanding the mechanisms underlying the control of tissue growth but also for developing the most optimal strategies to target this signaling pathway for clinical applications, such as to treat bone loss and muscle loss. In this regard, it will be important to elucidate the precise identities of the key ligands involved in regulating bone homeostasis as well as the precise receptors and other components utilized by these ligands for signaling in both muscle and bone. Moreover, FST is only one of multiple extracellular binding proteins that are capable of binding and inhibiting these ligands, and although considerable work has been done in examining the roles of these binding proteins in muscle, much less has been reported with respect to bone. Understanding the extent to which specific regulatory and signaling components are shared between bone and muscle will be especially important given the extensive ongoing effort among pharmaceutical and biotechnology companies to target this signaling pathway to treat patients with muscle loss and metabolic diseases (for a review, see ref. 52), as some of these therapeutic approaches and agents could also be useful to treat bone loss, including conditions characterized by comorbid bone and muscle loss.

The magnitude of the effect that we observed upon targeting the type 1 receptors in osteoblasts reveals the enormous inherent capacity for bone growth that is normally kept in check by this signaling pathway, and in many respects these findings are reminiscent of the massive increases in muscle mass that we observed upon targeting these same receptors in myofibers (22). These findings demonstrate that ligands capable of signaling through these receptors normally function to limit growth of muscle and bone and raise the question as to the extent to which signaling through this pathway may also limit growth of other tissues. Bullough originally proposed the term "chalone" to describe hypothetical circulating negative growth regulators that function to control tissue size (53). MSTN seems to fulfill all the essential criteria for a chalone for skeletal muscle (54, 55), and our findings raise the possibility that a similar regulatory mechanism with shared signaling components may be operating in other tissues as well.

Materials and Methods

All animal experiments were carried out in accordance with protocols that were approved by the Institutional Animal Care and Use Committees at the Jackson Laboratory, University of Connecticut School of Medicine, and Johns Hopkins University School of Medicine. Mice carrying floxed alleles for *Fst* (33), *Acvr2* (44), *Acvr2b* (35), *Alk4* (22), *Alk5* (56), and *Inhba* (57) have been described previously. Individual muscles were dissected and weighed from both sides of 10-wk-old mice, and the average weight was used for each muscle. Circulating protein levels were determined on acid-activated serum samples by enzyme-linked immunosorbent assay using the LSBio F13187 Kit (FST) and R&D Systems DGDF80 Kit (MSTN). Serial sections (15 μm) were cut transversely through the widest point of the gastrocnemius and triceps muscles using a cryostat. Fiber diameters were measured (as the shortest distance across each fiber passing through the midpoint) from hematoxylin and eosin–stained sections. Measurements were carried out on 250 fibers per muscle, and all data for a given genotype were pooled. Fiber type analysis was carried out using antibodies BA-D5, SC-71, and BF-F3 for myosin heavy chains type I, IIa, and IIb, respectively (58), obtained from the Developmental Studies Hybridoma Bank developed under the auspices of the National Institute of Child Health and Human Development and maintained by the University of Iowa. Nile red staining was carried out as described (59). Fluorescence was quantified using ImageJ on images taken with a Nikon Ti Eclipse wide-field microscope. RNA-seq, DXA scan, and micro-CT analyses were carried out as described previously (45). RNA extraction and analysis by real-time qPCR were performed as described previously (40). Histological and RNA-seq analyses were carried out on tissues isolated from male mice so that comparisons could be made with *F66* mice, which carry an *Fst*-overexpressing transgene located on the Y chromosome (24).

Data Availability. All study data are included in the article and/or *SI Appendix*.

ACKNOWLEDGMENTS. This research was supported by NIH Grants R01AR060636 (to S.-J.L.) and R01AG052962 (to S.-J.L.) and by funds from UConn Health (E.L.G.-L. and S.-J.L.) and Connecticut Children's (E.L.G.-L.). Follistatin and inhibin/activin mutant mouse models were created with the support of NIH Grant R01HD032067 (to M.M.M.). While at Johns Hopkins, S.-J.L. was supported by generous gifts from Michael and Ann Hankin, Partners of Brown Advisory, and James and Julieta Higgins.

1. A. C. McPherron, A. M. Lawler, S.-J. Lee, Regulation of skeletal muscle mass in mice by a new TGF-β superfamily member. *Nature* **387**, 83–90 (1997).
2. A. C. McPherron, S.-J. Lee, Double muscling in cattle due to mutations in the myostatin gene. *Proc. Natl. Acad. Sci. U.S.A.* **94**, 12457–12461 (1997).
3. L. Grobet *et al*., A deletion in the bovine myostatin gene causes the double-muscled phenotype in cattle. *Nat. Genet.* **17**, 71–74 (1997).
4. R. Kambadur, M. Sharma, T. P. L. Smith, J. J. Bass, Mutations in myostatin (GDF8) in double-muscled Belgian Blue and Piedmontese cattle. *Genome Res.* **7**, 910–916 (1997).
5. A. Clop *et al*., A mutation creating a potential illegitimate microRNA target site in the myostatin gene affects muscularity in sheep. *Nat. Genet.* **38**, 813–818 (2006).
6. D. S. Mosher *et al*., A mutation in the myostatin gene increases muscle mass and enhances racing performance in heterozygote dogs. *PLoS Genet.* **3**, e79 (2007).
7. Q. Lv *et al*., Efficient generation of myostatin gene mutated rabbit by CRISPR/Cas9. *Sci. Rep.* **6**, 25029 (2016).
8. H. Gu *et al*., Establishment and phenotypic analysis of an Mstn knockout rat. *Biochem. Biophys. Res. Commun.* **477**, 115–122 (2016).
9. K. Wang *et al*., CRISPR/Cas9-mediated knockout of myostatin in Chinese indigenous Erhualian pigs. *Transgenic Res.* **26**, 799–805 (2017).
10. Z. He *et al*., Use of CRISPR/Cas9 technology efficiently targetted goat myostatin through zygotes microinjection resulting in double-muscled phenotype in goats. *Biosci. Rep.* **38**, BSR20180742 (2018).
11. M. Schuelke *et al*., Myostatin mutation associated with gross muscle hypertrophy in a child. *N. Engl. J. Med.* **350**, 2682–2688 (2004).
12. S.-J. Lee, A. C. McPherron, Regulation of myostatin activity and muscle growth. *Proc. Natl. Acad. Sci. U.S.A.* **98**, 9306–9311 (2001).
13. J. J. Hill *et al*., The myostatin propeptide and the follistatin-related gene are inhibitory binding proteins of myostatin in normal serum. *J. Biol. Chem.* **277**, 40735–40741 (2002).
14. J. J. Hill, Y. Qiu, R. M. Hewick, N. M. Wolfman, Regulation of myostatin in vivo by growth and differentiation factor-associated serum protein-1: A novel protein with protease inhibitor and follistatin domains. *Mol. Endocrinol.* **17**, 1144–1154 (2003).
15. Y.-S. Lee, S.-J. Lee, Regulation of GDF-11 and myostatin activity by GASP-1 and GASP-2. *Proc. Natl. Acad. Sci. U.S.A.* **110**, E3713–E3722 (2013).
16. K. Kondás, G. Szláma, M. Trexler, L. Patthy, Both WFIKKN1 and WFIKKN2 have high affinity for growth and differentiation factors 8 and 11. *J. Biol. Chem.* **283**, 23677–23684 (2008).
17. R. S. Thies *et al*., GDF-8 propeptide binds to GDF-8 and antagonizes biological activity by inhibiting GDF-8 receptor binding. *Growth Factors* **18**, 251–259 (2001).
18. N. M. Wolfman *et al*., Activation of latent myostatin by the BMP-1/tolloid family of metalloproteinases. *Proc. Natl. Acad. Sci. U.S.A.* **100**, 15842–15846 (2003).
19. S.-J. Lee, Genetic analysis of the role of proteolysis in the activation of latent myostatin. *PLoS One* **3**, e1628 (2008).
20. S.-J. Lee *et al*., Regulation of muscle growth by multiple ligands signaling through activin type II receptors. *Proc. Natl. Acad. Sci. U.S.A.* **102**, 18117–18122 (2005).
21. F. Morvan *et al*., Blockade of activin type II receptors with a dual anti-ActRIIA/IIB antibody is critical to promote maximal skeletal muscle hypertrophy. *Proc. Natl. Acad. Sci. U.S.A.* **114**, 12448–12453 (2017).
22. S.-J. Lee *et al*., Functional redundancy of type I and type II receptors in the regulation of skeletal muscle growth by myostatin and activin A. *Proc. Natl. Acad. Sci. U.S.A.* **117**, 30907–30917 (2020).

23. A. Rebbapragada, H. Benchabane, J. L. Wrana, A. J. Celeste, L. Attisano, Myostatin signals through a transforming growth factor β-like signaling pathway to block adipogenesis. *Mol. Cell. Biol.* **23**, 7230–7242 (2003).
24. S.-J. Lee, Quadrupling muscle mass in mice by targeting TGF-β signaling pathways. *PLoS One* **2**, e789 (2007).
25. S.-J. Lee *et al*., Regulation of muscle mass by follistatin and activins. *Mol. Endocrinol.* **24**, 1998–2008 (2010).
26. E. Latres *et al*., Activin A more prominently regulates muscle mass in primates than does GDF8. *Nat. Commun.* **8**, 15153 (2017).
27. J. L. Chen *et al*., Specific targeting of TGF-β family ligands demonstrates distinct roles in the regulation of muscle mass in health and disease. *Proc. Natl. Acad. Sci. U.S.A.* **114**, E5266–E5275 (2017).
28. N. Ueno *et al*., Isolation and partial characterization of follistatin: A single-chain Mr 35,000 monomeric protein that inhibits the release of follicle-stimulating hormone. *Proc. Natl. Acad. Sci. U.S.A.* **84**, 8282–8286 (1987).
29. T. Nakamura *et al*., Activin-binding protein from rat ovary is follistatin. *Science* **247**, 836–838 (1990).
30. N. Ling *et al*., Pituitary FSH is released by a heterodimer of the beta-subunits from the two forms of inhibin. *Nature* **321**, 779–782 (1986).
31. K. Sugino *et al*., Molecular heterogeneity of follistatin, an activin-binding protein. Higher affinity of the carboxyl-terminal truncated forms for heparan sulfate proteoglycans on the ovarian granulosa cell. *J. Biol. Chem.* **268**, 15579–15587 (1993).
32. M. M. Matzuk *et al*., Multiple defects and perinatal death in mice deficient in follistatin. *Nature* **374**, 360–363 (1995).
33. C. J. Jorgez, M. Klysik, S. P. Jamin, R. R. Behringer, M. M. Matzuk, Granulosa cell-specific inactivation of follistatin causes female fertility defects. *Mol. Endocrinol.* **18**, 953–967 (2004).
34. A. C. McPherron, T. V. Huynh, S.-J. Lee, Redundancy of myostatin and growth/differentiation factor 11 function. *BMC Dev. Biol.* **9**, 24–32 (2009).
35. S.-J. Lee *et al*., Role of satellite cells versus myofibers in muscle hypertrophy induced by inhibition of the myostatin/activin signaling pathway. *Proc. Natl. Acad. Sci. U.S.A.* **109**, E2353–E2360 (2012).
36. T. Hinoi *et al*., Mouse model of colonic adenoma-carcinoma progression based on somatic Apc inactivation. *Cancer Res.* **67**, 9721–9730 (2007).
37. Y. Komiya *et al*., Mouse soleus (slow) muscle shows greater intramyocellular lipid droplet accumulation than EDL (fast) muscle: Fiber type-specific analysis. *J. Muscle Res. Cell Motil.* **38**, 163–173 (2017).
38. D. Pette, R. S. Staron, Cellular and molecular diversities of mammalian skeletal muscle fibers. *Rev. Physiol. Biochem. Pharmacol.* **116**, 1–76 (1990).
39. S. Schiaffino, C. Reggiani, Fiber types in mammalian skeletal muscles. *Physiol. Rev.* **91**, 1447–1531 (2011).
40. Y.-S. Lee, T. V. Huynh, S. J. Lee, Paracrine and endocrine modes of myostatin action. *J. Appl. Physiol. (1985)* **120**, 592–598 (2016).
41. A. Koncarevic *et al*., A soluble activin receptor type IIb prevents the effects of androgen deprivation on body composition and bone health. *Endocrinology* **151**, 4289–4300 (2010).
42. C. S. Chiu *et al*., Increased muscle force production and bone mineral density in ActRIIB-Fc-treated mature rodents. *J. Gerontol. A Biol. Sci. Med. Sci.* **68**, 1181–1192 (2013).
43. P. Bialek *et al*., A myostatin and activin decoy receptor enhances bone formation in mice. *Bone* **60**, 162–171 (2014).
44. B. C. Goh *et al*., Activin receptor type 2A (ACVR2A) functions directly in osteoblasts as a negative regulator of bone mass. *J. Biol. Chem.* **292**, 13809–13822 (2017).
45. S.-J. Lee *et al*., Targeting myostatin/activin A protects against skeletal muscle and bone loss during spaceflight. *Proc. Natl. Acad. Sci. U.S.A.* **117**, 23942–23951 (2020).
46. M. Zhang *et al*., Osteoblast-specific knockout of the insulin-like growth factor (IGF) receptor gene reveals an essential role of IGF signaling in bone matrix mineralization. *J. Biol. Chem.* **277**, 44005–44012 (2002).
47. M. N. Elkasrawy, M. W. Hamrick, Myostatin (GDF-8) as a key factor linking muscle mass and bone structure. *J. Musculoskelet. Neuronal Interact.* **10**, 56–63 (2010).
48. M. M. Matzuk *et al*., Functional analysis of activins during mammalian development. *Nature* **374**, 354–356 (1995).
49. C. E. Winbanks *et al*., The bone morphogenetic protein axis is a positive regulator of skeletal muscle mass. *J. Cell Biol.* **203**, 345–357 (2013).
50. R. Sartori *et al*., BMP signaling controls muscle mass. *Nat. Genet.* **45**, 1309–1318 (2013).
51. J. W. Lowery, V. Rosen, The BMP pathway and its inhibitors in the skeleton. *Physiol. Rev.* **98**, 2431–2452 (2018).
52. S.-J. Lee, Targeting the myostatin signaling pathway to treat muscle loss and metabolic dysfunction. *J. Clin. Invest.* **131**, e148372 (2021).
53. W. S. Bullough, The control of mitotic activity in adult mammalian tissues. *Biol. Rev. Camb. Philos. Soc.* **37**, 307–342 (1962).
54. S.-J. Lee, Regulation of muscle mass by myostatin. *Annu. Rev. Cell Dev. Biol.* **20**, 61–86 (2004).
55. S.-J. Lee, Extracellular regulation of myostatin: A molecular rheostat for muscle mass. *Immunol. Endocr. Metab. Agents Med. Chem.* **10**, 183–194 (2010).
56. J. Larsson *et al*., Abnormal angiogenesis but intact hematopoietic potential in TGF-beta type I receptor-deficient mice. *EMBO J.* **20**, 1663–1673 (2001).
57. S. A. Pangas *et al*., Intraovarian activins are required for female fertility. *Mol. Endocrinol.* **21**, 2458–2471 (2007).
58. S. Schiaffino *et al*., Three myosin heavy chain isoforms in type 2 skeletal muscle fibres. *J. Muscle Res. Cell Motil.* **10**, 197–205 (1989).
59. S. D. Fowler, P. Greenspan, Application of Nile red, a fluorescent hydrophobic probe, for the detection of neutral lipid deposits in tissue sections: Comparison with oil red O. *J. Histochem. Cytochem.* **33**, 833–836 (1985).